

Beam steering characteristics in high-power quantum-cascade lasers emitting at $\sim 4.6\ \mu m$

Yong-Qiang Sun(孙永强), Jin-Chuan Zhang(张锦川), Feng-Min Cheng(程凤敏), Chao Ning(宁超), Ning Zhuo(卓宁), Shen-Qiang Zhai(翟慎强), Feng-Qi Liu(刘峰奇), Jun-Qi Liu(刘俊岐), Shu-Man Liu(刘舒曼), and Zhan-Guo Wang(王占国)

Citation: Chin. Phys. B, 2021, 30 (**3**): 034211. DOI: 10.1088/1674-1056/abd6fe
Journal homepage: http://cpb.iphy.ac.cn; http://iopscience.iop.org/cpb

What follows is a list of articles you may be interested in

Random-injection-based two-channel chaos with enhanced bandwidth and suppressed time-delay signature by mutually coupled lasers: Proposal and numerical analysis

Shi-Rong Xu(许世蓉), Xin-Hong Jia (贾新鸿), Hui-Liang Ma(马辉亮), Jia-Bing Lin(林佳兵), Wen-Yan Liang(梁文燕), and Yu-Lian Yang(杨玉莲)

Chin. Phys. B, 2021, 30 (**1**): 014203. DOI: 10.1088/1674-1056/abb228

Research progress in terahertz quantum-cascade lasers and quantum-well photodetectors

Zhi-Yong Tan(谭智勇), Wen-Jian Wan(万文坚), Jun-Cheng Cao(曹俊诚)

Chin. Phys. B, 2020, 29 (**8**): 084212. DOI: 10.1088/1674-1056/aba945

Polarization control and tuning efficiency of tunable vertical-cavity surface-emitting laser with internal-cavity sub-wavelength grating

Xiao-Long Wang(王小龙), Yong-Gang Zou(邹永刚), Zhi-Fang He(何志芳), Guo-Jun Liu(刘国军), Xiao-Hui Ma(马晓辉)

Chin. Phys. B, 2020, 29 (**8**): 084208. DOI: 10.1088/1674-1056/ab9442

High gain fiber-solid hybrid double-passing end-pumped Nd: YVO_4 picosecond amplifier with high beam quality

Xueyan Dong(董雪岩), Pingxue Li(李平雪), Shun Li(李舜), Dongsheng Wang(王东生)

Chin. Phys. B, 2020, 29 (**5**): 054207. DOI: 10.1088/1674-1056/ab8218

Evaluation of polarization field in InGaN/GaN multiple quantum well structures by using electroluminescence spectra shift

Ping Chen(陈平), De-Gang Zhao(赵德刚), De-Sheng Jiang(江德生), Jing Yang(杨静), Jian-Jun Zhu(朱建军), Zong-Shun Liu(刘宗顺), Wei Liu(刘炜), Feng Liang(梁锋), Shuang-Tao Liu(刘双韬), Yao Xing(邢瑶), Li-Qun Zhang(张立群)

Chin. Phys. B, 2020, 29 (**3**): 034206. DOI: 10.1088/1674-1056/ab6967

RAPID COMMUNICATION

Beam steering characteristics in high-power quantum-cascade lasers emitting at ~ 4.6 μm*

Yong-Qiang Sun(孙永强)[1,2], Jin-Chuan Zhang(张锦川)[1,†], Feng-Min Cheng(程凤敏)[1,3], Chao Ning(宁超)[1,2], Ning Zhuo(卓宁)[1], Shen-Qiang Zhai(翟慎强)[1], Feng-Qi Liu(刘峰奇)[1,2,3,‡], Jun-Qi Liu(刘俊岐)[1,2], Shu-Man Liu(刘舒曼)[1,2], and Zhan-Guo Wang(王占国)[1,2]

[1] *Key Laboratory of Semiconductor Materials Science, Institute of Semiconductors, Chinese Academy of Sciences, Beijing Key Laboratory of Low Dimensional Semiconductor Materials and Devices, Beijing* 100083, *China*

[2] *Center of Materials Science and Optoelectronics Engineering, University of Chinese Academy of Sciences, Beijing* 100049, *China*

[3] *Beijing Academy of Quantum Information Sciences, Beijing* 100193, *China*

(Received 26 October 2020; revised manuscript received 16 December 2020; accepted manuscript online 28 December 2020)

A beam steering effect of high-power quantum cascade (QC) lasers emitting at ~ 4.6 μm was investigated. The continuous wave (CW) output power of an uncoated, 6-mm-long, 7.5-μm-wide buried-heterostructure QC laser at 25 °C was as high as 854.2 mW. The maximum beam steering angle was offset by $\pm 14.2°$ from the facet normal (0°) in pulsed mode. The phenomenon was judged explicitly by combining the diffraction limit theory and Fourier transform of the spectra. It was also verified by finite element method software simulation and the calculation of two-dimensional (2D) effective-index model. The observed steering is consistent with a theory for coherence between the two lowest order lateral modes. Therefore, we have established an intrinsic linkage between the spectral instabilities and the beam steering by using the Fourier transform of the spectra, and further presented an extremely valid method to judge the beam steering. The content of this method includes both three equidistant peak positions in the Fourier transform of the spectra and the beam quality located between once the diffraction limit (DL) and twice the DL.

Keywords: beam steering, quantum cascade lasers, fourier transform of the spectra, 2D effective-index model

PACS: 42.55.Px, 85.65.+h, 42.30.–d, 95.85.Hp **DOI:** 10.1088/1674-1056/abd6fe

1. Introduction

High power and high beam quality have always been the goals pursued by mid-infrared lasers. Currently, the quantum cascade (QC) lasers,[1] whose optical gain amplification derives from quantum-well intersubband transitions, have exhibited breakthrough progress toward these goals.[2–5] Additionally, the high power of this kind laser is frequently accompanied by nonlinear effects. This effect will cause many novel phenomena, which also have a great impact on the device. Beam steering is one of such nonlinear effects, which will have a huge impact on any system that requires relatively precise pointing.[6] For example, it not only affects the long-distance accurate detection of explosives by the laser through backscatter spectroscopy, but also stands as a huge obstacle for the directional infrared countermeasure (DIRCM).[6–8] Nevertheless, it is also possibly to be deliberately controlled[9] and used to perform laser projection by adjusting or scanning the direction of the laser beam.[10,11] Therefore, the origin of the beam steering effects has to be understood so that QC lasers can be better applied. Although the experimental evidence for beam steering in QC lasers has been reported and generally attributed to the interference of transverse modes[6,12] and spatial hole burning induced by higher lateral modes,[7] few studies have been done to explicitly establish an intrinsic linkage between the spectral instabilities and the beam steering and to explore the valuable criterion of the phase locking between the two lowest transverse modes when the beam steering happens.

In this paper, we combine the results of the spectrum, beam quality, and the Fourier transform spectrum based on the earlier ones[6,7,10] to suggest a method to directly judge the phase locking. The intrinsic linkage between the spectral instabilities and the beam steering is also explicitly expounded based on the Fourier transform spectrum. Then according to the theoretical calculation of a 2D effective-index model and finite element method software simulation, the theoretically calculated far field is obtained which is completely consistent with our experimental results.

2. Device materials design and waveguide structures

The QC laser wafer was grown on an n-doped (Si, 2×10^{17} cm^{-3}) InP substrate by solid-source molecu-

*Project supported by the National Basic Research Program of China (Grant Nos. 2018YFA0209103 and 2018YFB2200504), the National Natural Science Foundation of China (Grant Nos. 61991430, 61774146, 61790583, 61674144, and 61774150), and the Key Projects of the Chinese Academy of Sciences (Grant Nos. 2018147, YJKYYQ20190002, QYZDJ-SSW-JSC027, and XDB43000000).

†Corresponding author. E-mail: zhangjinchuan@semi.ac.cn

‡Corresponding author. E-mail: fqliu@semi.ac.cn

© 2021 Chinese Physical Society and IOP Publishing Ltd

lar beam epitaxy (MBE) based on a two-phonon resonance design, which is identical to that in Ref. [13]. The active core includes 30 stages of strain-compensated $In_{0.669}Ga_{0.331}As/In_{0.362}Al_{0.638}As$ quantum wells and barriers.[14] The entire structure is as follows: 3.0 μm lower cladding layer (Si, 2.2×10^{16} cm^{-3}), 30 active/injector stages, 0.3 μm-thick n-$In_{0.53}Ga_{0.47}As$ layer (Si, 4×10^{16} cm^{-3}), 2.4 μm (InP) upper cladding layer (Si, 2.2×10^{16} cm^{-3}), and 0.6 μm cap layer (Si, 5×10^{18} cm^{-3}). The layer sequence of one period, starting from the injection barrier is as follows (thickness in nanometers): 3.8/1.2/1.3/4.3/1.3/3.8/1.4/3.6/2.2/2.8/1.7/2.5/1.8/2.2/1.9/ 2.1/2.1/2.0/2.1/1.8/2.7/1.8, $In_{0.362}Al_{0.638}As$ barrier layers in bold, $In_{0.669}Ga_{0.331}As$ quantum well layers in roman, and doped layers (Si, 1.5×10^{17} cm^{-3}) were underlined. The specific structure of the device dies in details is shown in Figs. 1(a) and 1(b).

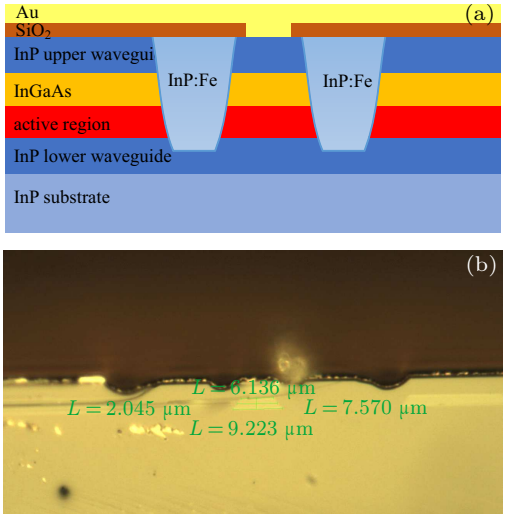


Fig. 1. (a) Schematic two-dimensional representation of the device G709. (b) The structure of G709 under a high-power optical microscope.

The epi-wafer was etched into a double-channel waveguide laser. First a 300 nm thick SiO_2 layer was deposited by plasma enhanced chemical vapor deposition (PECVD) as a mask for filling semi-insulating InP:Fe for better heat dissipation around the ridge. And a 450 nm thick SiO_2 layer was deposited for insulation, and electrical contact was provided by a Ti/Au layer deposited by electron beam evaporation. An additional 4 μm thick gold layer was electroplated to further improve the heat dissipation. After thinning down to about 140 μm, a Ge/Au/Ni/Au metal contact layer was deposited on the substrate side of the wafer. The waveguides were cleaved into 6-mm-long bars, and the facet of sample G709 was uncoated for the measurement of edging emitting power. Finally, the lasers were mounted epilayer side-down on a diamond heat-sink with indium solder, which were subsequently soldered on copper heat sinks.

3. Analysis of experimental results and model establishment verification

The lasers were tested after wire bonding, and mounting on a holder containing a thermoelectric cooler (TEC) to monitor the heat-sink temperature. The measurements were performed using a Fourier transform infrared (FTIR) spectrometer with 0.125 cm^{-1} resolution in rapid scan mode. The output optical power was collected by a calibrated thermopile detector, which was put in front of the laser front facet without any efficiency correction.

3.1. Analysis of experimental results

Figure 2 shows the typical power–current (*P–I*) curves of sample G709, with 6 to 14 μs current pulses at a repetition rate of 50 kHz and the heat-sink temperature 25 °C. During the test interval, to avoid damage, the lasers were not tested to the maximum operating current in this configuration. Its maximum output power exceeded 704 mW (on double facet) over a broad range of current, and the results of threshold current and dynamic range are similar. Additionally, the continuous wave (CW) light–current–voltage (*L–I–V*) curves of the sample G709 at the heat-sink temperature 25 °C are shown. Within the tested current range, the working voltage range was 6.543 V–11.054 V and its maximum double output power reached 854.2 mW.

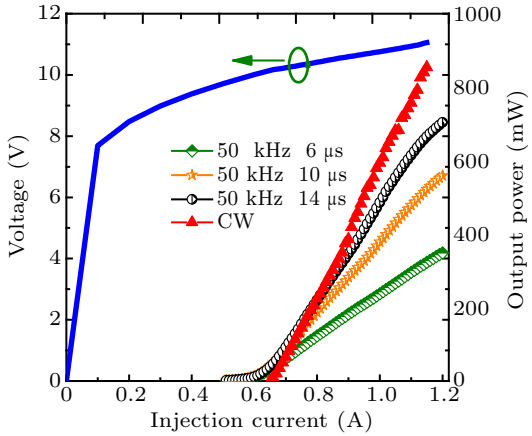


Fig. 2. Typical power–current curves of sample G709, with 14 μs current pulses at a repetition rate of 50 kHz and the heat-sink temperature 25 °C. It also shows the CW light–current–voltage curves of the sample G709 at the heat-sink temperature 25 °C.

Figure 3(a) shows the far-field patterns of the device at 25 °C along the ridge-width direction at different injection current. The far-field at 0.5 A exhibits a Gaussian-like distribution. As the current increases from 0.6 A to 0.9 A, the shoulder peaks distributed on both sides in the far field not only gradually enhance, but also irregularly deflect to the left and right directions. Especially in the range of 1.0 A–1.2 A, the far-field peak position undergoes a significant turning, known as the beam steering.[6] It should be noted that the maximum intensity peak of the beam in the far field is offset by +14.2° and

−14.2° from the facet normal (0°) at 1.0 A and 1.2 A, respectively. The facet normal (0°) is used as the zero coordinate of the far-field. The diffraction limit (DL) angle of the fundamental mode at the full-width at half-maximum (FWHM) is 46° according to the single-slit diffraction theory. In the entire test interval, the FWHM increases from 47° ± 0.5° (≈ 1.02 DL) at 0.5 A to 60° ± 0.5° (≈ 1.3 DL) at 1.2 A. Therefore, the far-field at high current could not be a pure fundamental transverse mode. Then perhaps the reason for this beam steering is that the two lowest transverse modes with slightly different effective refractive indexes are coherent, and the phase difference between the modes is constant. Furthermore, varying the current induces substantial angular steering of the output, which is usually accompanied by a significant qualitative change in the spectral characteristics.[6,10]

Figure 3(b) shows that the range of the spectrum gradually broadens from 0.031 μm at 0.5 A to 0.146 μm at 0.9 A. However, the longitudinal mode range of the spectrum suddenly decreases in the range of 1.0 A–1.2 A. It is possible that the increase of the current causes the gain hole-burning effect. Additionally, the spectrum of 1.0 A shows that although a significant small range of widening and multiple longitudinal modes exist around 4.72 μm, it also can be clearly observed that there are a series of relatively small and uniform longitudinal modes in the 4.65 μm–4.70 μm range. Nevertheless, when the laser is energized at 1.1 A and 1.2 A, the optical intensities of the multi-longitudinal mode distributed in this spectrum range are minimal caused by obvious hole-burning in the gain space.

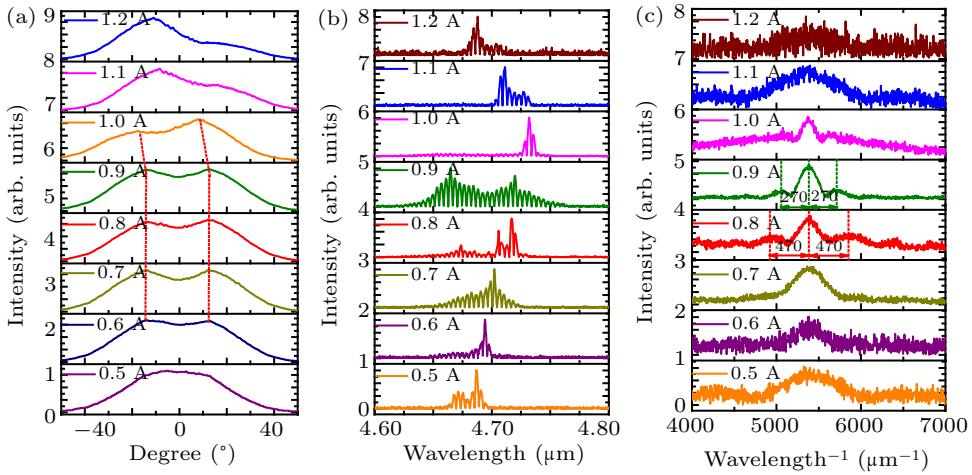


Fig. 3. (a) Measured far-field intensity distributions of the device at driving currents of 0.5, 0.6, 0.7, 0.8, 0.9, 1.0, 1.1, and 1.2 A (from bottom to top) in pulsed mode at the heat-sink temperature 25 °C. (b) Emission spectra for the $\lambda = 4.65$ μm QCL at $T = 25$ °C. (c) Fourier transforms of the spectra. The laser is driven by pulsed current from 0.5 A to 1.2 A at a repetition rate of 50 kHz. The pulse duration is 10 μs.

In order to further verify that the beam steering may be caused by the coherence of the two transverse modes. We performed Fourier transform of the spectra. Figure 3(c) shows that there are two situations in the Fourier analysis over a broad range of injection currents, either only showing one peak at a certain current, or showing three closely adjacent and equally spaced peaks.[12] And there is no observation of multiple peaks that are closely adjacent and spaced differently at a certain current. This shows no incoherence between transverse modes in this range.[6,12] At the same time, the far-field profiles under most currents [Fig. 3(a)] obviously do not show a completely consistent Gaussian distribution, indicating that these far-fields at high current should not be a pure fundamental transverse mode. Furthermore, since most of the far-fields FWHM are between once the DL and twice the DL in the 0.5 A–1.2 A interval, it cannot be considered that these far-fields only contain the first-order mode. As a result, it is natural to attribute them to that the two lateral lowest modes with slightly different effective refractive indices are coherent. This demonstrates the phase locking of the two lowest modes to judge the occurrence of the beam steering.

Finally, COMSOL simulations and theoretical model calculations are performed to further verify the rationality of the judgement and experimental results.

3.2. Model establishment and verification

The modes are simulated by solving the Maxwell's equations with a 2D finite-element method software. According to the simulation, the two lowest transverse modes can coexist in the laser cavity, as shown in Fig. 4(a), where the TM0 and TM1 modes are represented in the bottom panel and top panel, respectively.

It is noted that the stripe width for the double-channel devices typically varies from 6.1 μm at the top of the active region to 9.2 μm at the bottom, while for the buried heterostructure the average waveguide width is 7.5 μm. The reason why high-order modes appear in such a narrow ridge is that the thinner waveguide layer on the active area of the device causes plasmon loss. Therefore, it is very effective to produce a high beam quality by appropriately increasing the thickness of the

top waveguide layer and relatively reducing the ridge width. On the basis of the results, figure 4(b) shows the calculated far-field profiles by taking various phase difference (-0.6π to 0.6π) between the basic 0th lateral mode and the 1st lateral mode.

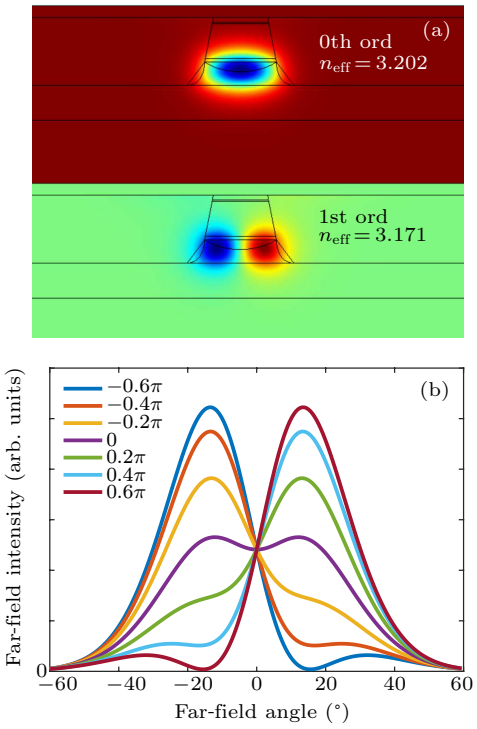


Fig. 4. (a) Calculated 2D optical mode distribution for the quantum cascade laser, 0th lateral mode (top panel) and 1st lateral mode (bottom panel). (b) Theoretical far-field profiles for a 7.5-μm-wide QCL emitting at 4.65 μm, for a series of phase differences (Φ) ranging from -0.6π to 0.6π. The ratio of photon densities in the two lowest order modes is assumed to be $P_0/P_1 = 3:4$.

From a 2D effective-index model, we assume that the ratio of the photon density of the fundamental mode to the first-order mode is $P_0/P_1 = 3:4$. The optical field of the whole superposition is approximately[6,15–17]

$$E(x,z) = \sqrt{P0}E_0(x)\,\mathrm{e}^{-\mathrm{j}\beta_0 z} + \sqrt{P1}E_1(x)\,\mathrm{e}^{-\mathrm{j}\beta_1 z}, \qquad (1)$$

where β_0 and β_1 represent the propagation constants of the fundamental and first-order modes, respectively. The relationship between the two coefficients simulated in COMSOL is $\beta_0 - \beta_1 \approx 0.031k_0$, where $k_0 = 2\pi/\lambda$. E_0 and E_1 represent the near fields of the fundamental mode and the first-order mode, which can be obtained from COMSOL.

Therefore, if we assume that the aligned phase is at the back facet (phase difference = 0),[6] then the phase difference between the two on the cavity surface can be calculated according to the following formula:

$$\Phi(z = L_{\rm c}) = \frac{2\pi\Delta n L_{\rm c}}{\lambda}, \qquad (2)$$

where Δn is the difference between the effective refractive indices of the two near-field modes, $L_{\rm c}$ is the cavity length of the laser, and λ is the wavelength of the laser. Through this calculation is ideal, the initial far-field experimental result at 0.6 A is consistent with the theoretical calculation of $\Phi = 0$, indicating that there is no constant phase in the two modes at the beginning. By this method, we estimate that the phase difference between the two lateral modes is around 0.2π at 1.0 A or -0.2π at 1.1 A, and that the calculated far field profile beam steering angle is around 13.5° or −13.5°, which fairly well agrees with the experimental value of 14.2° or −14.2°.

3.3. Conclusion and perspectives

In summary, we explain the intrinsic linkage between the spectral instabilities and the beam steering and report a valuable criterion consisting of the analysis of the Fourier transform of the spectra and beam quality to judge the phase difference locking of two modes. Furthermore, our model for 2D interference between the two lowest order lateral modes reproduces the experimental finding. That is, a given device can switch between strong steering in either direction or no steering when the operating conditions (phase difference) are varied. This sufficiently verifies that the criterion of beam steering given in this paper is extremely effective.

Acknowledgment

The authors would like to thank Ping Liang and Ying Hu for their help in device processing.

References

[1] Faist J, Capasso F, Sivco D L, Sirtori C, Hutchinson A L and Cho A Y 1994 *Science* **264** 553
[2] Bai Y, Darvish S R, Slivken S, Zhang W, Evans A, Nguyen J and Razeghi M 2008 *Appl. Phys. Lett.* **92** 101105
[3] Razeghi M, Slivken S, Bai Y, Gokden B and Darvish S R 2009 *New J. Phys.* **11** 125017
[4] Lyakh A, Maulini R, Tsekoun A, Go R, Pflugl C, Diehl L, Wang Q J, Capasso F and Patel C K N 2009 *Appl. Phys. Lett.* **95** 141113
[5] Bai Y, Bandyopadhyay N, Tsao S, Slivken S and Razeghi M 2011 *Appl. Phys. Lett.* **98** 181102
[6] Bewley W W, Lindle J R, Kim C S, Vurgaftman I, Meyer J R, Evans A J, Yu J S, Slivken S and Razeghi M 2005 *IEEE J. Quantum Electron.* **41** 833
[7] Yang Q, Kinzer M, Fuchs F, Hugger S, Hinkov B, Bronner W, Lösch R, Aidam R and Wagner J 2012 *Phys. Status Solidi (c)* **9** 302
[8] Tholl H D, Wagner J, Rattunde M, Hugger S and Fuchs F 2010 *SPIE Security + Defence*, 12 October, 2010, Toulouse, France, 78360Q
[9] Slivken S, Wu D H and Razeghi M 2017 *Sci. Rep.* **7** 8472
[10] Kinzer M, Fuchs F, Hugger S, Hinkov B, BronnerW, Loe-sch R, Aidam R, Yang Q K and Tholl H D 2010 *SPIE Security + Defence*, 12 October, 2010, Toulouse, France, 78360R
[11] Lee S, Alexander J W and Gerry G O 2001 *Photonics West 2001 - LASE*, 20 June, 2001, San Jose, CA, United States, 4272
[12] Yu N F, Diehl L, Cubukcu E, Bour D, Corzine S, Hofler, G, Wojcik A K, Crozier K B, Belyanin A and Capasso F 2009 *Phys. Rev. Lett.* **102** 013901
[13] Liu F Q, Li L, Wang L J, Liu J Q, Zhang W, Zhang Q D, Liu W F, Lu Q Y and Wang Z G 2009 *Appl. Phys. A* **97** 527
[14] Evans A, Darvish S R, Slivken S, Nguyen J, Bai Y and Razeghi M 2007 *Appl. Phys. Lett.* **91** 071101
[15] Schemmann M F C, van der Poel C J, van Bakel B A H, Ambrosius H P M M, Valater A, van den Heijkant J A M and Acket G A 1995 *Appl. Phys. Lett.* **66** 920
[16] Tan G L, Mand R S and Xu J M 1997 *IEEE J. Quantum Electron.* **33** 1384
[17] Guthrie J, Tan G L, Ohkubo M, Fukushima T, Ikegami Y, Ijichi T, Irikawa M, R. S. Mand R S and Xu J M 1994 *IEEE Photon. Technol. Lett.* **6** 1409